CALIBRATION OF A TERRESTRIAL FULL WAVEFORM LASER SCANNER

Preston J. Hartzell
Craig L. Glennie
Department of Civil and Environmental Engineering
University of Houston
Houston, TX 77204
pjhartzell@uh.edu
clglennie@uh.edu

David C. Finnegan
Cold Regions Research and Engineering Lab
Hanover, NH 03755
david.finnegan@usace.army.mil

ABSTRACT

Recent advances in Light Detection And Ranging (LiDAR) enable digital acquisition and storage of the entire waveform of backscattered laser pulse energy. Pre-requisites for extracting target radiometric and geometric properties via waveform analysis include defining a model for accurately determining peaks in the return energy waveform and a method for transforming waveform peak amplitudes to absolute reflectance values. The development of a system response waveform model and reflectance calibration curves for a terrestrial LiDAR sensor is described and the results compared to expected values. Our analysis shows that overall system response varies considerably over the dynamic range of the instrument, requiring the development of an empirical template to properly estimate the expected system response at a given input signal amplitude. Finally, it is shown that the relationship between target absolute reflectance and raw waveform peak amplitude varies considerably with range to target, requiring a distance dependent model for conversion of raw amplitudes to absolute reflectance values.

KEYWORDS: calibration, full waveform, light detection and ranging (LiDAR), reflectance

INTRODUCTION

Airborne and ground-based Light Detection And Ranging (LiDAR) systems have become a standard mechanism for acquiring dense high-precision topography and three dimensional models. Traditional LiDAR sensors provide a series of discrete returns, which represent peaks in the backscattered illumination. The sensors also typically report the magnitude (intensity) of these returns, normally based on an arbitrary scaling that is dependent upon the output pulse power and the instrument hardware. Recent technological advancements, however, allow the recording of the entire echo waveform of the backscattered illumination at high sampling rates (500 MHz-2 GHz). This technology, termed Full Waveform LiDAR (FWL), provides a new ability to enhance pulse peak detection through post processing and further quantify additional information about the imaged scene by parametric and volumetric analysis of the sampled backscattered illumination.

To date, waveform analysis techniques have primarily been limited to the detection of return amplitude peaks for 3D coordinate definition (Mallet & Bretar, 2009; Wagner et al., 2006; Parrish, 2007; Chauve et al., 2007; Roncat, Bergauer, & Pfeifer, 2011; Mallet et al., 2009), with more recent use of return pulse widths for vegetation filtering for digital terrain model creation (Wagner et al., 2008a; Mucke, Briese, & Hollaus, 2010). The methods investigated have mainly focused on fitting parametric models to the returned waveform to reliably extract object range estimates, and to increase the number and speed at which peaks are detected. These methods are especially applicable in cluttered reflector environments where the laser response from multiple overlapping surfaces results in complex return waveforms and individual peaks can be difficult to discriminate. A large body of literature exists detailing the process of fitting waveforms with a given parametric model, and a summary of different modeling approaches to the raw waveform signals can be found in (Mallet et al., 2009). In general, it has been concluded that the use of Gaussian or generalized Gaussian models is an acceptable method for peak detection and estimation. However, it is difficult to conclude this with certainty, because, to date, the majority of the FWL research conducted

has relied upon airborne sensors and measurements. In these cases, the pulse detection methods can be heuristically checked against the digitized waveform, but leave no opportunity to control the imaged scene within the laser pulse cone of diffraction to ensure that the pulse detection methodology is accurately modeling the backscattered radiation and extracting the correct peaks at the proper locations. Gaussian pulse modeling may therefore not be appropriate for all laser scanners, especially for FWL sensors whose overall system response does not show the same Gaussian behavior and stability that the current expensive airborne FWL scanners exhibit. In addition, as discussed in (Pfennigbauer & Ullrich, 2010; Ullrich & Pfennigbauer, 2011), Gaussian modeling is not appropriate over the entire dynamic range of current systems, especially for high amplitude signals. In these cases, alternative methodology for modeling the system response to more accurately extract target information is required.

As stated above, most modern laser scanning systems give an intensity value, which is a unitless measurement of the relative peak signal strength of the return pulse. The scale and resolution of intensity values varies between sensor manufacturers. The expected backscattered signal strength can be estimated for a laser system using a form of the LiDAR link equation that accounts for the major elements of the LiDAR system (Cossio et al., 2010). If we assume a collimated beam and diffusely reflecting surface, the amount of photoelectron energy at the LiDAR detector can be given as:

$$\eta_s = \eta_q \eta_r \frac{E_t}{h\nu} \cdot \rho_\lambda \cos(\alpha) \frac{A_r}{\pi R^2} \cdot \left[\exp(-\beta_{e,\lambda} R)\right]^2 \tag{1}$$

where η_q is the detector quantum efficiency, η_r is the receiver optical efficiency, E_t is the transmitted energy of the pulse in joules, h is Planck's constant, υ is the laser frequency in Hz, ρ_λ is the wavelength dependent surface reflectance, α is the angle of incidence on the surface, A_r is the collection area of the receiver aperture, $\beta_{\varepsilon,\lambda}$ is the atmospheric extinction coefficient, and R is the range to the target surface. For a given LiDAR system,

$$C = \eta_q \eta_r \frac{E_t}{h\upsilon} \cdot \frac{A_r}{\pi} \approx CONSTANT \tag{2}$$

and therefore the return energy is given by

$$\eta_s = C \cdot \frac{\rho_\lambda \cos(\alpha)}{R^2} \cdot \left[\exp(-\beta_{e,\lambda} R)\right]^2 \tag{3}$$

This implies that for a given LiDAR system the variation in return signal strength is directly influenced by atmospheric effects, range to target, surface reflectance, and target incidence angle of the incoming radiation. Obviously, the influence of range can easily be removed, and if we assume that the atmosphere is stable over the time period of a survey, the return waveform amplitude should potentially be able to give us information regarding incidence angle and the reflective properties of the target.

This paper describes the development of empirical system response waveform templates spanning the dynamic range of a terrestrial laser scanner for which Gaussian fitting was found to be inappropriate. The templates were derived from controlled FWL measurements to calibrated targets of known reflectance, thereby providing the ability to transform subsequent observed peak waveform amplitudes to absolute imaged target reflectance values, i.e., radiometric calibration. Knowledge of the target geometry used for creating the system response templates also provides a basis for future analysis of waveform deviation from the template model for correlation to target properties. The waveform templates should also allow for more accurate range estimation by utilizing the observed system response in full waveform decomposition algorithms.

DATASET DESCRIPTION

VZ-400 and Reflectance Standards Description

For the purposes of this study, the University of Houston has acquired a VZ-400 tripod laser scanner manufactured by Riegl of Horn, Austria. Specifications for the VZ-400 are given in Table 1. The VZ-400 scanner utilized in this study has been upgraded with a firmware modification by the manufacturer that allows for full

Table 1. VZ-400 Specifications		
Parameter	Long Range Mode	High Speed Mode
Effective Pulse Rate (Hz)	42,000	122,000
Max. Range (reflectivity = 90%)	600	350
Max. Range (reflectivity = 20%)	280	160
Range Accuracy (mm)	5	
Range Precision (mm)	3	
Beam Divergence (mrad)	0.3	
Angular Resolution (º)	0.0005	
Laser Wavelength (nm)	1550	

waveform recording of the backscattered laser energy. The return energy is digitized at a 500 MHz rate, or a sample every 2 nanoseconds. A typical return waveform measured with the VZ-400 from a flat surface with a zero incidence angle is given in Figure 1.

An examination of the waveform profile in Figure 1 introduces two significant issues for modeling the waveform response of the VZ-400 laser scanner. First, due to both the narrow outgoing pulse width (FWHM of approx. 5-7 ns), and the low digitization rate (2 ns samples), there are very few points captured on the return pulse – perhaps only 5 or 6. This makes it difficult to accurately and reliably fit a model to the return pulse shape. Second, the return pulse clearly does not have a Gaussian distribution, as there is a significant tail in the return pulse. This indicates that Gaussian modeling will likely not lead to accurate and reliable estimates for the target properties encapsulated in the return waveforms. The manufacturer of this laser uses a process they call online waveform processing with the VZ-400 in order to estimate return locations in real-time. For this processing, rather than fitting Gaussian models, they have stored a series of templates of the system response at intervals across the instrument dynamic range. See (Pfennigbauer & Ullrich, 2010) for a discussion of the manufacturer's implementation.

The full waveform mode of the VZ-400 only provides the user with information about the backscattered laser energy. Very little information about the internal properties of the laser scanner or pulse is recorded (for example, the shape of the outgoing pulse is not known). Therefore, in order to properly analyze the system response, develop templates for range estimation and deviation analysis, and calibrate the laser returns to provide absolute reflectance estimates, we are required to perform measurements to known reflectance standards in known geometric configurations (Wagner et al., 2008b). For this purpose, three 12" by 12" Spectralon calibrated reflectance targets were purchased from Labsphere. The three targets have a nominal reflectance of 99%, 50%, and 20%, respectively, in the visible spectrum, and are shown in Figure 2. However, the actual reflectance of each of these targets is computed into the mid-infrared by the manufacturer (Labsphere, 2013), and from these reflectance profiles we can determine their actual reflectance at 1550 nm (the wavelength of the VZ-400) as 99%, 62%, and 30%.

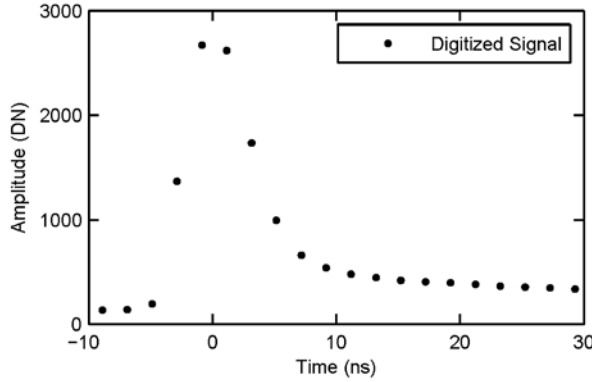

Figure 1. Typical waveform response for the VZ-400.

Figure 2. Labsphere Spectralon Reflectance Targets.

Data Collection

In order to capture the entire dynamic range of the VZ-400 and to provide sufficiently dense sampling to reliably determine the system response templates and absolute reflectance response, a comprehensive set of measurements to the known reflectance standards was collected over multiple days on the campus of the University of Houston. The distance between the scanner and the reflective targets was varied from 2 m to 260 m in the following increments: 2-32 m in 2 m increments, 35-70 m in 5 m increments, 80-140 m in 10 m increments, and 160-260 m in 20 m increments. At each distance, several thousand waveform samples were collected from each

target with an approximate 0º incidence angle. As shown in Figure 2, the 99% reflectance standard was mounted on a pan and tilt tripod which allowed it to be rotated at each distance to also collect waveforms with 20°, 40°, and 60° angles of incidence.

The instrument was operated in high speed mode (see Table 1) for all measurements. The VZ-400 uses a high and low power channel to accommodate the large dynamic range of return energy (Riegl, 2012); only low channel waveforms are considered here, as the high channel was rarely used when imaging the reflectance standards. To simplify illustration and analysis, only those observations beyond approximately 10 m are presented, thereby avoiding most near-field attenuation effects (Pfennigbauer & Ullrich, 2010). Studies of discrete LiDAR intensities with respect to distance and incidence angle at shorter ranges can be found in (Kukko, Kaasalainen, & Litkey, 2008; Kaasalainen et al., 2009; Kaasalainen et al., 2011). It is noted that the addition of the short range observations to the waveform and reflectance models described in this paper is easily accomplished.

ANALYIS AND DISCUSSION

Full Waveform Modeling

In order to calculate template waveforms that can be used to determine expected system response (at normal incidence) to pulses of varying amplitude, the dataset described above was analyzed. The several thousand return waveforms collected at each distance were aligned using the temporal peak location obtained from a simple cubic spline fit to each waveform. Note that the spline is being used to align the waveforms to create a more dense representation of the system response for a given return pulse amplitude, not as a functional model for extracting target properties, such as in (Roncat, Bergauer, & Pfeifer, 2011). For example, the pulses for the 99% reflectance standard collected at 32 m with normal incidence are shown in Figure 3. Prior to selecting the cubic spline, several other functional models, including Gaussian variants, were fit to the waveforms but found to produce inconsistent alignment results. This is a further indication that Gaussian pulse-fitting is not appropriate for the VZ-400.

Each set of aligned waveforms was used to create an average waveform, and the average waveforms generated from each target combined to create a template of the expected return waveform shape over the dynamic range of the VZ-400. The template model for 99% reflective Spectralon at 0° incidence is given in Figure 4. An examination of Figure 4 shows that the return waveform at high amplitudes is significantly different from those at lower amplitudes, and has a much slower extinction. However, the change of the waveform shape over the entire dynamic range is quite smooth. The development of this template provides a simple reference for the predicted system response for a given return amplitude. This will allow for a more accurate estimation of the target location and possibly enable the extraction of additional target properties from deviations in the actual measured return waveform from the expected system response.

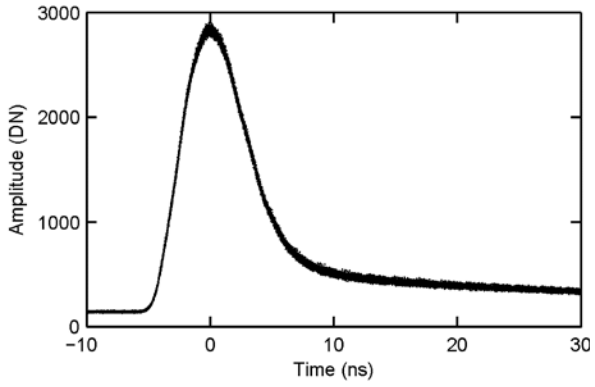

Figure 3. Several thousand return pulse waveforms from 99%

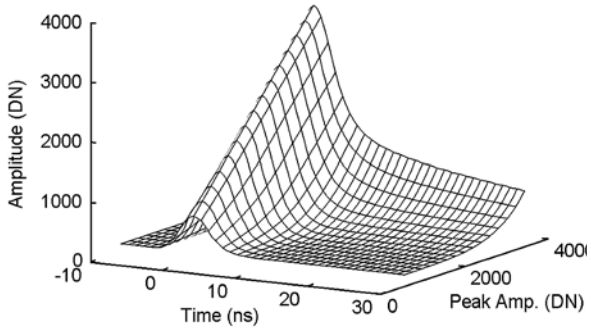

Figure 4. 3D plot of return waveforms over dynamic range of VZ-400 from 99% Spectralon, 0° incidence.

Incidence Angle

As previously mentioned, during the data collection at each distance, the angle of incidence for the 99% reflective Spectralon target was varied from 0° to 60° in 20° increments to determine the influence of incidence angle on the backscattered pulse. The variation in the return waveform with varying incidence angle at two distances is given in Figure 5 and a plot of peak waveform amplitude with respect to range for the 40° and 60° incidence angles is given in Figure 6. As demonstrated by Equation (1), we would expect the amplitude of the return pulse to be decreased in proportion to the cosine of the angle of incidence. This relationship appears to hold at longer target distances (approximately 160 m and above, as evidenced by Figure 5 and Figure 6), but does not hold true for shorter target distances. This may partially be because the Spectralon targets do not behave as perfectly diffuse Lambertian surfaces in the backscattering direction (Papetti et al., 2007), but it is unclear how their diffusivity is influenced by distance. (Riegl, 2012) indicates that non-linearity exists in the signal detection process of the Riegl instrument for stronger returned echo signals, which may be a contributing factor at shorter ranges.

It is also interesting to note that the increased incidence angle does not alter the width of the return pulse significantly (Figure 7). This is due to the fact that the beam from the VZ-400 has a relatively small divergence, and therefore the extent of the incident laser light on the target, even at larger angles of incidence, is not significant enough to spread the return energy profile at the sensor within the 500 MHz sampling rate of the VZ-400 waveform digitizer's resolution. In addition, (Lin & Mills, 2010) reports that surface roughness is the dominant influence in expanded pulse widths for small-footprint airborne LiDAR, which may also be the case for terrestrial LiDAR sensors.

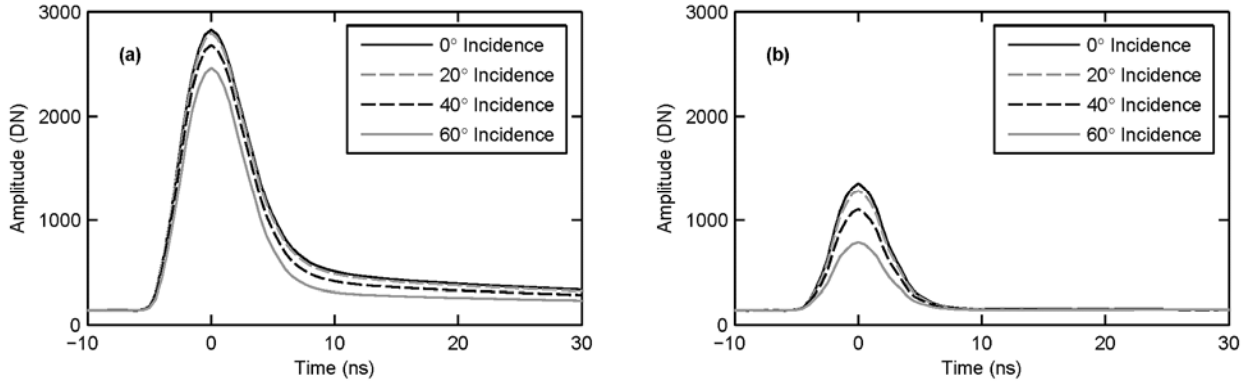

Figure 5. Variation in return waveform shape due to changing incidence angle from 99% reflective Spectralon target at 32 m **(a)** and 160 m **(b)**.

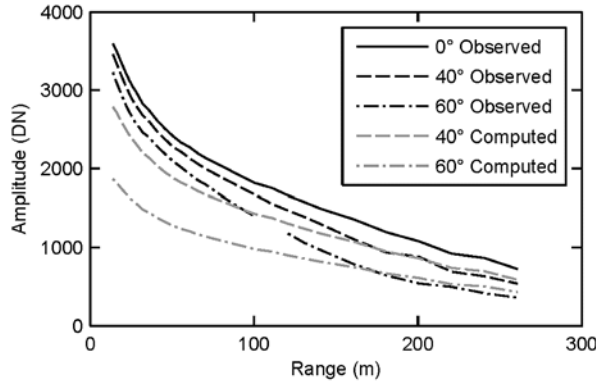

Figure 6. Measured and computed amplitude versus range curves for 99% Spectralon at 40° and 60° incidence angles (20° incidence omitted for clarity).

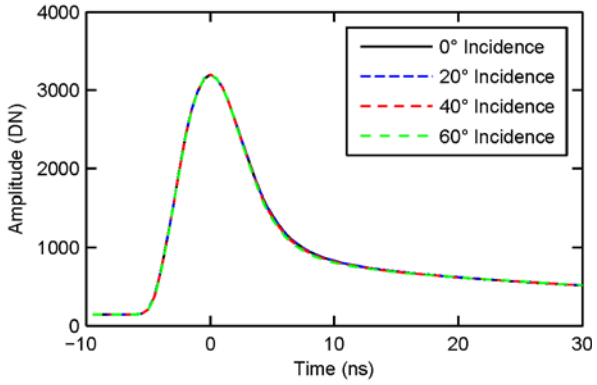

Figure 7. Equal peak amplitude waveforms from 99% Spectralon observed at 0°, 20°, 40°, and 60° incidence angles.

Absolute Reflectance Modeling

The Riegl VZ-400 laser scanner is unique in the LiDAR industry in that instead of providing an un-calibrated peak amplitude as the return intensity measurement, it returns a more physically meaningful pair of values which are referred to as "calibrated amplitude" and "relative reflectance" (Pfennigbauer & Ullrich, 2010). The calibrated amplitude measurement is given in dB over the detection threshold of the instrument for its entire dynamic range. However, because this amplitude value, as shown in Equation (1), is highly dependent on the range to the target, Riegl goes one step further to compute a "relative reflectance", which is the ratio of the calibrated amplitude of the target to the calibrated amplitude of a white reflectance standard at the same target range. This use of relative reflectance allows a more seamless combination of scan data from different ranges and different fields of view. However, although it provides a more normalized view of intensity, it does not directly give an absolute reflectance value. Therefore, to get a sense of absolute reflectance, the amplitude of the returns from 99%, 50%, and 20% Spectralon samples (99%, 62%, and 30% reflectance at 1550 nm) versus range to target was analyzed. These results are shown in Figure 8.

The graph in Figure 8(a) shows in dark lines the amplitude of the response versus distance for 99%, 62% and 30% (at 1550 nm) Spectralon. The gray lines on this graph represent amplitudes of 62% and 30% of the observed amplitude from the 99% Spectralon (the base digitizer noise level was accommodated in the calculations); i.e., these curves represent the expected reflectance of the 62% and 30% panels, if the instrument was providing peak waveform amplitudes proportional to proper absolute reflectance. An examination of the curves shows that the reflectance of the 62% and 30% panels is higher than expected for all ranges up to approximately 200 m. The convergence to expected values at longer ranges is similar to that shown in Figure 6 with respect to incidence angle, perhaps in part for similar reasons as mentioned previously. The graph in Figure 8(b) is the sample amplitude versus distance plotted on a log-log scale. The amplitude drop-off in this graph is approximately straight line up to about 100 meters, which shows that for the instrument the $1/R^2$-law is applicable, as is shown in (Pfennigbauer & Ullrich, 2010). However, beyond 100 meters the linear log-log relationship no longer holds. It is speculated that beyond 100 meters we begin to observe an additional decrease in amplitude due to atmospheric extinction.

Given the results in Figure 8 we have been able to develop an empirical absolute reflectance model for the scanner that will allow us to transform a full waveform peak amplitude measurement to an estimate of absolute reflectance by using an interpolation between the calibrated 99%, 62%, and 30% reflectance values at each distance. Future work will include the addition of observations to a 2% reflectance target and validation of the reflectance model to determine whether or not it can be used to accurately determine absolute reflectance of targeted objects.

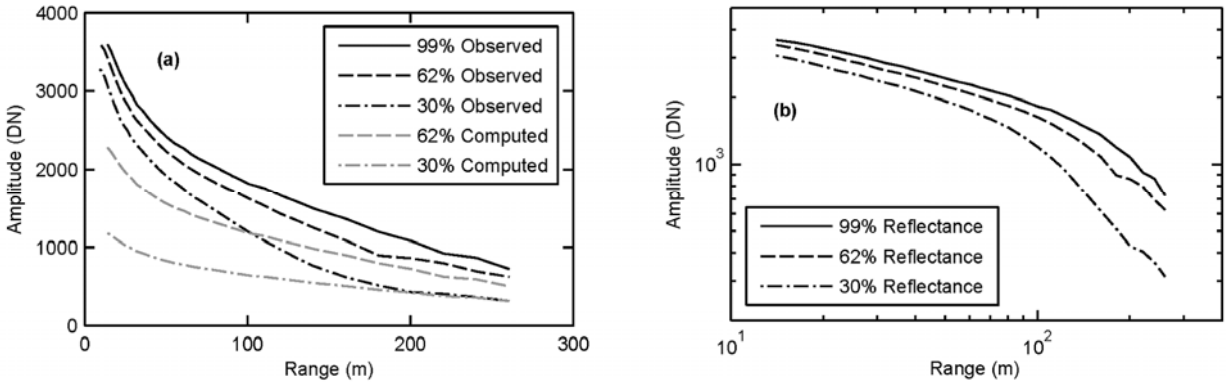

Figure 8. Amplitude versus range for Spectralon targets. Measured and computed reflectance curves are compared in **(a)**. The straight line portions of the reflectance curves on the log-log plot in **(b)** shows the power relationship between amplitude and range.

CONCLUSION

Although widely used, the Gaussian function is not an appropriate model for the VZ-400 system response due to the elevated waveform tail and changing waveform shape across the sensor's dynamic range. Therefore, a series of measurements to targets of known reflectance and geometry were used to develop a system response template for waveform peak modeling. The measurements were also used to develop calibration curves for transforming waveform peak amplitudes to absolute reflectance values

Future work will include validating the reflectance calibration curves with observations to additional reflectance standards, and examining deviations of observed waveforms from fitted template waveform models for potential correlation to target properties.

REFERENCES

Chauve, A. et al., 2007. Processing full-waveform lidar data: Modelling raw signals. In *International Archives of Photogrammetry, Remote Sensing and Spatial Information Sciences XXXVI (Part 3/W52)*. Espoo, Finland, pp. 102–107.

Cossio, T.K. et al., 2010. Predicting Small Target Detection Performance of Low-SNR Airborne Lidar. *IEEE Journal of Selected Topics in Applied Earth Observations and Remote Sensing*, 3(4), pp.672–688.

Kaasalainen, S. et al., 2009. Radiometric Calibration of Terrestrial Laser Scanners with External Reference Targets. *Remote Sensing*, 1(3), pp.144–158.

Kaasalainen, S. et al., 2011. Analysis of Incidence Angle and Distance Effects on Terrestrial Laser Scanner Intensity: Search for Correction Methods. *Remote Sensing*, 3(10), pp.2207–2221.

Kukko, A., Kaasalainen, S. & Litkey, P., 2008. Effect of incidence angle on laser scanner intensity and surface data. *Applied optics*, 47(7), pp.986–92.

Labsphere, 2013. Technical Guide, Reflectance Materials and Coatings, Labsphere Inc., North Sutton, NH, accessed Jan. 8, 2013, http://www.labsphere.com/uploads/technical-guides/a-guide-to-reflectance-materials-and-coatings.pdf.

Lin, Y. & Mills, J.P., 2010. Factors Influencing Pulse Width of Small Footprint , Full Waveform Airborne Laser Scanning Data. *Photogrammetric Engineering & Remote Sensing*, 76(1), pp.49–59.

Mallet, C. & Bretar, F., 2009. Full-waveform topographic lidar: State-of-the-art. *ISPRS Journal of Photogrammetry and Remote Sensing*, 64(1), pp.1–16.

Mallet, C. et al., 2009b. A stochastic approach for modelling airborne lidar waveforms. In *International Archives of Photogrammetry, Remote Sensing and Spatial Information Sciences XXXVIII (Part 3/8)*. pp. 201-206.

Mucke, W., Briese, C. & Hollaus, M., 2010. Terrain echo probability assignment based on full-waveform airborne laser scanning observables. In *International Archives of Photogrammetry, Remote Sensing and Spatial Information Sciences XXXVIII (Part 7A)*. Vienna, Austria, pp. 157–162.

Papetti, T.J. et al., 2007. Coherent backscatter: measurement of the retroreflective BRDF peak exhibited by several surfaces relevant to ladar applications. In *Proceedings of SPIE*, 6682, p.66820E–66820E–13.

Parrish, C., 2007. *Full-Waveform Lidar Data Using A 3d Wavelet-Based Approach*. Ph.D. thesis, Dept. of Civil Eng., University of Wisconsin.

Pfennigbauer, M. & Ullrich, A., 2010. Improving quality of laser scanning data acquisition through calibrated amplitude and pulse deviation measurement. In *SPIE Defense, Security & Sensing*. Orlando, Florida, paper #7684-53.

Riegl, 2012. Waveform Extraction Library, Riegl Laser Measurement Systems GmbH, Horn, Austria, printed Dec. 6, 2012.

Roncat, A., Bergauer, G. & Pfeifer, N., 2011. β-spline deconvolution for differential target cross-section determination in full-waveform laser scanning data. *ISPRS Journal of Photogrammetry and Remote Sensing*, 66(4), pp.418–428.

Ullrich, A. & Pfennigbauer, M., 2011. Categorisation of full waveform data provided by laser scanning devices. In *Electro-Optical Remote Sensing, Photonic Technologies, and Applications V*, vol. 8186, pp. 818609–818609–10.

Wagner, W. et al., 2006. Gaussian decomposition and calibration of a novel small-footprint full-waveform digitising airborne laser scanner. *ISPRS Journal of Photogrammetry and Remote Sensing*, 60(2), pp.100–112.

Wagner, W. et al., 2008a. 3D vegetation mapping using small-footprint full-waveform airborne laser scanners. *International Journal of Remote Sensing*, 29(5), pp.1433–1452.

Wagner, W et al., 2008b. Radiometric Calibration of Full-Waveform Small-Footprint Airborne Laser Scanners. In *International Archives of Photogrammetry, Remote Sensing and Spatial Information Sciences 37* (B1), pp. 163-168.